NACA

RESEARCH MEMORANDUM

INVESTIGATION OF AXIAL-FLOW FAN AND COMPRESSOR

ROTORS DESIGNED FOR THREE-DIMENSIONAL FLOW

By

A. Kahane

Langley Memorial Aeronautical Laboratory
Langley Field, Va.

NATIONAL ADVISORY COMMITTEE
FOR AERONAUTICS

WASHINGTON
May 2, 1947

NATIONAL ADVISORY COMMITTEE FOR AERONAUTICS

RESEARCH MEMORANDUM

INVESTIGATION OF AXIAL-FLOW FAN AND COMPRESSOR

ROTORS DESIGNED FOR THREE-DIMENSIONAL FLOW

By A. Kahane

SUMMARY

An investigation has been conducted to determine
whether three-dimensional flows may be efficiently uti-
lized in axial-flow fan and compressor rotors so that the
spanwise load distribution may be suitably varied to
obtain high pressure rise. Two rotors, one with approxi-
mately uniform and one with solid-body downstream
tangential-velocity distributions, were designed and
tested at the design blade angle. Radial surveys of total
pressure, static pressure, and flow angle were made
upstream and downstream of the test rotors through a
quantity-coefficient range. Tests of the solid-body
rotor were also conducted at a large value of tip clear-
ance.

The results indicated that the three-dimensional
flows may be utilized with high efficiency and that the
three-dimensional theory used in conjunction with two-
dimensional cascade data is sufficiently accurate for
design purposes. The tests also showed that the tip-
clearance losses of rotors highly loaded at the tips are
not excessive. The existing three-dimensional theory in
simplified form and an illustrative rotor design are
presented in appendixes.

INTRODUCTION

The conventional method of blade design for axial-
flow fans and compressors specified a free-vortex type
of blade loading, which is characterized by a flow
through the rotor disk that is essentially two-dimensional.
Tests of a series of free-vortex designed fans are
reported in reference 1; the experimental results

therein show excellent agreement with the theory. For
designs in which a high-pressure-rise rotor is required,
use of spanwise load distributions differing from the
free-vortex type may be desirable. Compressibility
effects may be appreciable, however, in the determination
of the most suitable load distribution of high-pressure-
rise rotors.

When the blade loading is different from the free-
vortex type, a three-dimensional flow may occur at
the fan; this flow results in a change of axial-velocity
distribution from upstream to downstream of the blading.
In order to design the rotor accurately, the axial
velocity at the blades must be known. The effect of
the blade load distribution on the axial-velocity profile
at a rotor and stator was initially determined in reference 2
by the solution of the Euler equations. Tests of low-
solidity fans are also reported in reference 2. No
attempt was made to load these fans highly at the tips
and, inasmuch as only total-pressure surveys were made,
only limited conclusions as to the applicability of the
theory to design could be drawn. An alternate method for
the determination of the actual velocity distribution at
a rotor in three-dimensional flow in terms of the flow
angles was presented in British reports of limited circu-
lation but the labor involved in the solution is excessive.

Two rotors with higher loading at the tips than
free-vortex-type blading have been designed and tested
in the Langley propeller-research-tunnel laboratory
to determine whether the three-dimensional theory may
be effectively used to design higher-pressure-rise
rotors. The rotors were designed for upstream velocities
which were both axial and uniform and for approximately
constant and "solid-body" downstream absolute tangential-
velocity distributions. (Solid-body notation indicates
a variation of tangential velocity directly proportional
to the radius.) Tests of each rotor were made at
the design blade angle through a range of quantity
coefficient. Radial surveys of total pressure, static
pressure, and flow angle were made upstream and down-
stream of each test rotor. Tests of the solid-body
rotor were also conducted at a large value of tip

clearance to determine whether the high pressure rise at the tip would adversely affect the tip losses.

The experimental results of the present investigation are given herein and are compared with theoretically predicted values. The three-dimensional theory in a simplified form is presented in appendix A, and a rotor design procedure is illustrated in a sample calculation in appendix B.

SYMBOLS AND COEFFICIENTS

c   blade chord, feet

B   number of blades

C_H total-pressure-rise coefficient $\left(\dfrac{\overline{\Delta H}}{\rho n^2 D^2}\right)$

c_l section lift coefficient based on mean relative velocity

C_p static-pressure-rise coefficient $\left(\dfrac{\overline{\Delta p}}{\rho n^2 D^2}\right)$

C_T torque coefficient $\left(\dfrac{T}{\rho n^2 D^5}\right)$

D   inside diameter of fan casing, feet

H   total pressure, pounds per square foot

ΔH total-pressure rise, pounds per square foot

$\overline{\Delta H}$ weighted average total-pressure rise (incompressible flow assumed), pounds per square foot

$$\left(\frac{2\pi}{Q}\int_{r_h}^{R} r\left(H_2 V_{a_2} - H_1 V_{a_1}\right)\,dr\right)$$

n   rotational speed, revolutions per second

p static pressure, pounds per square foot

Δp static-pressure rise, pounds per square foot

$\overline{\Delta p}$ weighted average static-pressure rise (incompressible flow assumed), pounds per square foot

$$\left(\frac{2\pi}{Q} \int_{r_h}^{R} r(p_2 V_{a_2} - p_1 V_{a_1})\, dr \right)$$

q_a effective axial dynamic pressure at fan, pounds per square foot

Q quantity rate of flow, cubic feet per second

Q/nD^3 quantity coefficient

r radius, feet

R radius to fan casing, feet

T torque, pound-feet

$$\left(2\pi \int_{r_h}^{R} \rho_2 u_2 V_{a_2} r^2\, dr \right)$$

u absolute tangential velocity, feet per second

V absolute velocity, feet per second

V_a effective axial velocity at fan, feet per second

x radius ratio (r/R)

α angle between effective relative entering air and chord line of blade, degrees

β stagger angle; angle between the effective relative entering air and fan axis, degrees

δ tangential-velocity parameter $(u/\omega R)$

η efficiency

η_H total-pressure-rise efficiency $\left(\dfrac{1}{2\pi} \dfrac{C_H}{C_T} \dfrac{Q}{nD^3} \right)$

η_p static-pressure-rise efficiency $\left(\dfrac{1}{2\pi} \dfrac{C_p}{C_T} \dfrac{Q}{nD^3} \right)$

θ effective turning angle, degrees

ρ mass density of air, slugs per cubic foot

σ solidity $(Bc/2\pi r)$

φ flow parameter $(V_a/\omega R)$

$\Delta\varphi$ increment of flow parameter along radius $(\Delta V_a/\omega R)$

ω rotor angular velocity, radians per second

Subscripts:

a   axial

A   a particular radius

B   a particular radius

h   hub

o   atmospheric

1   upstream of fan

2   downstream of fan

Bar over symbol indicates an average value.

THEORETICAL CONSIDERATIONS

Flow through a Rotor

In the conventional method of design of axial-flow fan and compressor blading, the blades are loaded radially so that no mutual interference exists between

adjacent blade elements. This loading is accomplished
by having the absolute tangential velocities in front of
and behind the fan vary inversely with the radius, or

$$u = \frac{\text{Constant}}{r}$$

Because of the analogy between this tangential-velocity
field and the radial variation of velocity due to a
line vortex situated on the fan axis, rotors designed
in such a manner are known as free-vortex rotors. The
flow through free-vortex blading in incompressible flow
is essentially two-dimensional in character; no radial
velocities occur in the flow field outside the boundary-
layer regions. In incompressible flow, therefore, the
axial velocities at a particular radius are the same
upstream and downstream of the fan when the flow area is
constant. A free-vortex rotor is also characterized by
a uniform total-energy rise across the annulus.

When the blades are loaded in a manner different
from the free-vortex manner, radial velocities may be
induced in the flow through them, and, if so, this flow
is therefore of a three-dimensional nature. It should
be pointed out that it is possible in some cases to obtain
a two-dimensional-type flow with non-free-vortex loaded
blading. Consider a rotor loaded so that the direction
of the radial velocities is outward. The flow streamlines
are therefore deflected outward. (See fig. 1.) The flow
reaches a radial equilibrium behind the fan when the
pressure forces balance the centrifugal forces of the
rotating flow. The axial velocities have increased at
the outer radii and decreased at the inner radii. Refer-
ence 2 shows that, upon assumption of an infinite number
of blades, an infinitesimally thin rotor disk, and a
system of trailing vortices that extends downstream to
infinity in concentric cylinders, the effective axial
velocity at the blade V_a is the mean of the axial
velocities at points upstream and downstream where
equilibrium exists. This relation is expressed in the
following equation:

$$V_a = \frac{V_{a_1} + V_{a_2}}{2} \tag{1}$$

The determination of the axial-velocity distribution
at the blades, as given in reference 2, is presented in
a simplified form for a rotor and stator in appendix A.
The theory has been presented for an incompressible
fluid, but the result is identical for a compressible
fluid. The application of the theory is illustrated
in a sample three-dimensional rotor design in appendix B.

A higher pressure rise may be obtained by loading
the rotor higher at the tips than the corresponding
free-vortex loaded rotor. The increase of total-pressure
rise theoretically obtainable by loading a rotor, the
upstream flow of which is uniform and axial, so that the
tangential-velocity distribution downstream is either
of the uniform or solid-body type is shown in figure 2,
wherein the more heavily loaded rotors are compared with
a free-vortex loaded rotor that has the same value of
tangential velocity at the hub. The solid-line curves
are plots of the approximate formulas derived in
appendix C. The dashed curve was computed exactly for
a solid-body rotor operating at $\frac{\omega R}{V_{a_1}} = 1.75$, with

$\left(\frac{u_2}{V_{a_1}}\right)_h = 0.60$, by weighting the total-pressure rise

with the velocity distribution determined from equation (7).
Results obtained with exact and approximate methods were
in good agreement. Figure 2 indicates that extremely
large increases of pressure rise may be obtained with
a solid-body rotor at the lower hub-tip radius ratios.

Application of Cascade Data to Three-Dimensional-Flow

Blading Design

Because of the two-dimensional nature of the flow
through a free-vortex fan, the flow through the rotating
blades at a given radius is analogous to the two-
dimensional flow through the corresponding cascade of
airfoils (reference 3). The static-pressure rise and
the total-pressure rise realized in an incompressible
frictionless fluid may be written as functions of the
stagger angle β and the turning angle θ; they are
(see fig. 3(a)):

$$\frac{\Delta p}{q_a} = \tan^2\beta - \tan^2(\beta - \theta)$$

$$\frac{\Delta H}{q_a} = \frac{\Delta p}{q_a} + \left(\frac{u_2}{V_a}\right)^2 - \left(\frac{u_1}{V_a}\right)^2 = \tan^2\beta - \tan^2(\beta - \theta) + \left(\frac{u_2}{V_a}\right)^2 - \left(\frac{u_1}{V_a}\right)^2$$

When the axial velocity varies through the blades, as in three-dimensional flow, the flow is no longer similar to that through a two-dimensional cascade. The actual flow could most closely be approximated in a cascade tunnel, in which the test-section flow area was varied by diverging or converging side walls. Cascade data of this nature, however, are not available at the present time. In the absence of complete experimental information use of two-dimensional cascade data should be possible with the qualification that the stagger and turning angles are to be computed relative to the mean axial velocity, as shown in figure 3(b). The equations for the static-pressure rise and the total-pressure rise are, accordingly,

$$\frac{\Delta p}{q_a} = \tan^2\beta - \tan^2(\beta - \theta) + \left(\frac{V_{a_1}}{V_a}\right)^2 - \left(\frac{V_{a_2}}{V_a}\right)^2 \qquad (2)$$

$$\frac{\Delta H}{q_a} = \frac{\Delta p}{q_a} + \left(\frac{u_2}{V_a}\right)^2 - \left(\frac{u_1}{V_a}\right)^2 - \left(\frac{V_{a_1}}{V_a}\right)^2 + \left(\frac{V_{a_2}}{V_a}\right)^2$$

$$= \tan^2\beta - \tan^2(\beta - \theta) + \left(\frac{u_2}{V_a}\right)^2 - \left(\frac{u_1}{V_a}\right)^2 \qquad (3)$$

APPARATUS

Test Setup

The general arrangement of the test setup, a modification of the equipment of reference 4, is shown in figures 4 and 5. The fan blades were mounted in the 24-blade hub used in the tests of reference 4. The power for the fan was supplied by a 25-horsepower, water-cooled, alternating-current electric motor.

The fan casing at the test section was of rolled and welded steel plate bored to a diameter of 21 inches. The radial-survey instruments were mounted in this casing 4 inches ahead of and behind the rotor center line and were spaced about 120° apart. The rear survey instrument was located about 1.4 chord lengths behind the blade trailing edges. The instruments (fig. 6) consisted of a total-pressure tube, a static-pressure tube, and a yaw head mounted in a single $\frac{1}{4}$-inch tube that could be moved along and rotated about a radial axis. A scale and calibrated knob permitted the reading of the radial position of the tube to 0.001 inch, and the angular position of the tube could be read on a protractor and vernier to 0.1°.

Preliminary tests with the bell inlet of reference 4 indicated that severe fluctuations of flow existed and that these fluctuations prevented accurate angular readings with the yaw heads. An inlet with a 10 to 1 area contraction and three screens was then installed and found satisfactory.

The diffuser and throttle downstream were the same as those used in the tests of reference 4.

Test Fans

The rotors investigated are designated fans 1, 2, and 2a. The tip clearance of fans 1 and 2 was about 0.015 inch. The tip clearance of fan 2a was about 0.063 inch; in other respects fan 2a was identical with fan 2. Each fan consisted of 24 blades of constant chord equal to 2.32 inches and of nominal span equal to $3\frac{1}{4}$ inches. The ratio of the hub and tip radii was 0.69. The solidity at the pitch section (located halfway between the inner and outer walls) was 1.0. The blade sections were of the 10-percent-thick NACA 65-series blower-blade sections investigated in cascade in references 3 and 5. Drawings of the blades are shown in figure 7 and the section ordinates are given in table I.

Fan 1 was designed for a constant section lift coefficient c_l of 0.7 along the blade at a value of the

design quantity coefficient Q/nD^3 of 0.587. This c_l
distribution corresponded to an approximately constant
absolute tangential-velocity distribution downstream of
the blades at the design point. A second fan with the
same solidity as that of fan 1 was designed for a solid-
body tangential-velocity distribution at a value of
Q/nD^3 of 0.587. Preliminary calculations indicated that
a slightly twisted blade with uniform section along
the span would give the desired result. For simplicity of
construction, therefore, fan 2 was built as a straight
blade with the NACA 65-(12)10 blower-blade section along
the span. The blade characteristics and theoretical
performance characteristics of fans 1 and 2 are presented
in figure 8.

TEST METHOD

Before the actual fan tests were made, the static-
pressure tube was calibrated to determine the interference
effects. The yaw-head zeros were determined by removing
the test fan, sealing the gap, and drawing air through the
setup with a blower.

The tests were conducted at a fan rotational speed
of about 3000 rpm. The quantity flow was regulated with
the exit throttle. At each of from 18 to 20 stations along
the radius, the front and rear survey tubes were rotated
until "null" readings were obtained on the U-tube manome-
ters connected to the yaw heads. Readings of total
pressure, static pressure, survey-tube radial position
and angle, wet- and dry-bulb temperatures, and rotational
speed were then taken. The barometer was read before and
after a run. Inasmuch as the speed of the drive motor
tended to vary during a test, readings were taken only
when the rotational speed was within ±10 rpm of that
specified for the test.

The power input was measured by the amount of
rotation put into the air. The quantity flow, the
total-pressure rise and the static-pressure rise were
determined by integration of the survey measurements.

The tests were conducted at a Reynolds number (based
on blade chord) of approximately 350,000 and a Mach number
of about 0.24. These values of Reynolds number and Mach
number were both based on mean relative velocity.

RESULTS AND DISCUSSION

Over-All Fan Characteristics

The fan-characteristic curves of the three configurations investigated are presented in figure 9. Comparison of the experimental coefficients at the design point $\left(\frac{Q}{nD^3} = 0.587\right)$ with the theoretically predicted coefficients of fans 1 and 2 are shown in the following table:

Coefficient	Fan 1		Fan 2	
	Theory	Experiment	Theory	Experiment
c_H	2.43	2.63	3.58	3.51
c_p	1.99	1.97	2.56	2.48
c_T	.240	.258	.352	.348
η_H	------	.935	------	.942
η_p	------	.718	------	.666

The agreement between experiment and theory is considered good. The high values of total-pressure efficiency obtained indicated that no large mixing loss is associated with the three-dimensional flow.

The effect of the increased tip clearance of fan 2a was to decrease the value of η_H at the design point about 3 percent. Fans loaded highly at the tips do not appear to be subject to excessive tip-clearance losses.

The surge points of fans 2 and 2a, as indicated by the smallest quantity coefficient at which data could be taken, occurred at values of Q/nD^3 of about 0.50 and 0.52, respectively. These values indicate that the effect of the increased tip clearance was to reduce the operating range of the fan.

Surveys

Fans 1 and 2.- The results of the surveys of fans 1
and 2 are presented in figures 10 and 11, respectively,
as plots of the radial distributions of the total and
static pressures in front of and behind the fans, the
tangential and axial velocities downstream of the blades,
and the stagger and turning angles, each at several values
of the quantity coefficient Q/nD^3.

The distribution of total pressure upstream of the
fans (figs. 10(a) and 11(a)) was essentially uniform
outside the boundary-layer region. The total-pressure
distributions downstream of the blades are characterized
by low-energy regions at the walls, which are the result
of losses due to secondary flows, tip clearance, and the
rotating hub. These distributions also indicate that
the blade loading is shifted toward the tips as the
quantity flow is decreased.

The static-pressure distributions upstream of the
fans (figs. 10(b) and 11(b)) were essentially uniform.
The sudden rise of static-pressure coefficient near the
boundaries appears to be the result of wall interference
on the static-pressure-tube reading. The static-pressure
gradient downstream of the rotor increases with decreasing
quantity coefficient. This increase is as expected, since
the static-pressure gradient when radial equilibrium is
attained (see equation (6)) is

$$\frac{dp_2}{dr} = \rho_2 \frac{u_2^2}{r}$$

and u_2 varies directly with the loading.

The survey measurements indicated that the tangential
velocities upstream of the rotor were essentially zero.
The tangential velocities downstream of fans 1 and 2
are presented in figures 10(c) and 11(c). The tangential
velocities downstream of fan 1 decrease generally with
distance from the inner wall, whereas the tangential
velocities downstream of fan 2 show a general increase
with distance from the inner wall.

The upstream total-pressure and static-pressure distributions of figures 10(a), 10(b), 11(a), and 11(b) indicate that the axial-velocity distribution ahead of the rotor was essentially uniform. Distributions of axial velocity downstream of fans 1 and 2 are presented in figures 10(d) and 11(d). The profiles are all characterized by low-velocity regions at the walls. At a value of Q/nD^3 of 0.710 the axial velocities downstream of fan 1 are essentially uniform. At values of Q/nD^3 less than 0.710 the axial velocities outside the boundary regions increase with distance from the inner wall, whereas the reverse is true for values of Q/nD^3 greater than 0.710. The axial velocities downstream of fan 2 increase with distance from the inner wall throughout the entire operating range. The axial-velocity gradients of fan 2 were larger than those of fan 1 inasmuch as the tips were more heavily loaded.

The stagger-angle distributions of fans 1 and 2 are presented in figures 10(e) and 11(e). The rise of stagger angle near the walls is associated with the axial-velocity defect in the boundary regions. In general, because of the steeper axial-velocity gradients of fan 2, the stagger-angle distributions of this fan are flatter than those of fan 1.

The turning-angle distributions of fans 1 and 2 are shown in figures 10(f) and 11(f). These distributions are characterized by a sharp increase and then a decrease of turning angle near the inner wall and a decrease near the outer wall. The rise of turning angle near the inner wall is probably the result of an increase of angle of attack on the blade section, which is caused by the low effective axial velocity in that region. The decrease of turning angle immediately adjacent to both walls occurs probably because of the predominating effect of the losses close to the wall. The turning angles of both fans decrease in general with distance from the inner wall, but the gradient is slight for fan 2.

Comparison of design-point experimental surveys with theory.- A comparison of the experimental survey results at the design point with the theoretically predicted

values is shown in figures 12(a) and 12(b) for fans 1
and 2, respectively. The downstream axial-velocity and
total-pressure-rise gradients obtained experimentally
with fan 1 differ slightly from those predicted because
of the deviation of the experimental and theoretical
tangential-velocity distributions. The downstream axial-
velocity, total-pressure-rise, and tangential-velocity
gradients obtained with fan 2 show good agreement with
the theoretical slopes outside the boundary regions. For
the hub-tip radius ratio of these tests $(x_h = 0.69)$ the
boundary-loss effects upon the total-pressure-rise and
axial-velocity distributions appear to be secondary to
the effect of load distribution. The agreement between
the theoretical and experimental values is considered
good and indicates that the three-dimensional theory may
effectively be used for design purposes.

Calculations of the downstream static-pressure
gradient at the design point of fans 1 and 2 were made
by use of the equation for radial equilibrium

$$p_{2_B} - p_{2_A} = \int_{r_A}^{r_B} \rho_2 \frac{u_2{}^2}{r} \, dr$$

and experimentally obtained values of tangential velocity.
These values are compared with the measured static-pressure
distributions in figure 13, the theoretical curve having
been arbitrarily placed so as to intersect the experi-
mental points at the center of the annulus. The resulting
good agreement indicates that radial equilibrium existed
at the rear survey station.

Effect of increased tip clearance.- The results of
the surveys of fan 2a are presented in figure 14. The
distributions are similar to those of fan 2 except for
slight irregularities near the outer wall. In figure 15
surveys of fans 2 and 2a are compared at a value of
Q/nD^3 of 0.586. The values for fan 2a in figure 15 were
obtained by interpolation. The increased tip clearance
decreased the total-pressure rise and downstream axial

velocities near the outer wall. Inasmuch as the quantity
coefficients were the same, the axial velocities downstream
were larger for fan 2a than for fan 2 throughout the
remainder of the annulus. This effect decreased the
angle of attack, the turning angle, and therefore the
total-pressure-rise coefficient in the inner region of the
annulus. The comparisons show that, for the tip clearances
investigated, the three-dimensional theory could be used
with similar accuracy for large and small tip clearances.

CONCLUSIONS

An investigation in the Langley propeller-research-
tunnel laboratory of two axial-flow rotors, one with
approximately uniform and one with solid-body downstream
tangential-velocity distributions indicated that:

1. High-efficiency axial-fan and compressor blading
may be designed incorporating three-dimensional flows;
the use of such flows allows variation of spanwise load
distribution to obtain higher pressure rise.

2. The three-dimensional theory used in conjunction
with two-dimensional cascade data is sufficiently accurate
for design purposes.

3. The tip-clearance losses of rotors loaded highly
at the tips are not excessive.

Langley Memorial Aeronautical Laboratory
    National Advisory Committee for Aeronautics
        Langley Field, Va.

APPENDIX A

DETERMINATION OF AXIAL-VELOCITY DISTRIBUTION

IN THREE-DIMENSIONAL FLOW THROUGH

A ROTOR AND STATOR

Consider the flow of an incompressible fluid through a rotor. The total-pressure rise of the flow in a stream tube may be expressed from Euler's turbine formula (reference 2) as

$$H_2 - H_1 = \eta_H \rho \omega r (u_2 - u_1) \tag{4}$$

In this equation the radial displacement of the stream tube is neglected. Inasmuch as

$$H_1 = p_1 + \frac{\rho}{2} V_{a_1}^2 + \frac{\rho}{2} u_1^2$$

and

$$H_2 = p_2 + \frac{\rho}{2} V_{a_2}^2 + \frac{\rho}{2} u_2^2$$

equation (4) can be written

$$p_2 - p_1 + \frac{\rho}{2} V_{a_2}^2 - \frac{\rho}{2} V_{a_1}^2 + \frac{\rho}{2} u_2^2 - \frac{\rho}{2} u_1^2 = \eta_H \rho \omega r (u_2 - u_1)$$

Differentiating this equation with respect to the radius results in

$$\frac{dp_2}{dr} - \frac{dp_1}{dr} + \rho V_{a_2} \frac{dV_{a_2}}{dr} - \rho V_{a_1} \frac{dV_{a_1}}{dr} + \rho u_2 \frac{du_2}{dr} - \rho u_1 \frac{du_1}{dr} =$$

$$\rho \omega \left[\frac{d(\eta_H r u_2)}{dr} - \frac{d(\eta_H r u_1)}{dr} \right] \tag{5}$$

If stations 1 and 2 are chosen at points where radial equilibrium of the flow exists, the pressure gradient of the rotating-air particles balances the centrifugal force due to rotation, or (see reference 2)

$$\frac{dp}{dr} = \rho \frac{u^2}{r} \tag{6}$$

Substitution of equation (6) in equation (5) results in

$$V_{a_2} \, dV_{a_2} = \omega \left[d(\eta_H r u_2) - d(\eta_H r u_1) \right] + V_{a_1} \, dV_{a_1} + u_1 \, du_1 - u_2 \, du_2$$

$$+ \frac{u_1^2}{r} \, dr - \frac{u_2^2}{r} \, dr$$

Integration between the limits of radii r_A and r_B gives

$$V_{a_{2_B}}^2 - V_{a_{2_A}}^2 = 2\omega \left[(\eta_H r)_B (u_{2_B} - u_{1_B}) - (\eta_H r)_A (u_{2_A} - u_{1_A}) \right]$$

$$+ \left(V_{a_{1_B}}^2 - V_{a_{1_A}}^2 \right) + \left(u_{1_B}^2 - u_{1_A}^2 \right) - \left(u_{2_B}^2 - u_{2_A}^2 \right)$$

$$+ 2 \int_{r_A}^{r_B} \frac{u_1^2}{r} \, dr - 2 \int_{r_A}^{r_B} \frac{u_2^2}{r} \, dr \tag{7}$$

Equation (7) indicates that, when the conditions upstream
of the rotor and the downstream tangential-velocity distri-
bution are known, the difference in axial velocities at
two radial positions downstream of the fan may be deter-
mined. With the introduction of the dimensionless
parameters

$$\varphi = \frac{V_a}{\omega R} \qquad x = \frac{r}{R} \qquad \vartheta = \frac{u}{\omega R}$$

equation (7) becomes

$$\varphi_{2_B}^2 - \varphi_{2_A}^2 = 2 \left[(\eta_H x)_B (\vartheta_{2_B} - \vartheta_{1_B}) - (\eta_H x)_A (\vartheta_{2_A} - \vartheta_{1_A}) \right]$$

$$+ \left(\varphi_{1_B}^2 - \varphi_{1_A}^2 \right) + \left(\vartheta_{1_B}^2 - \vartheta_{1_A}^2 \right) - \left(\vartheta_{2_B}^2 - \vartheta_{2_A}^2 \right)$$

$$+ 2 \int_{r_A}^{r_B} \frac{\vartheta_1^2}{x} \, dx - 2 \int_{r_A}^{r_B} \frac{\vartheta_2^2}{x} \, dx \tag{8}$$

When a functional relationship exists between ϑ and x,
the integrals in equation (8) may be evaluated analytically;
otherwise, a graphical integration can be performed. The
integrals may also be evaluated with good accuracy by con-
sidering the area under the curve a trapezoid, or

$$2 \int_{r_A}^{r_B} \frac{\vartheta^2}{x} \, dx = \left[\left(\frac{\vartheta^2}{x} \right)_B + \left(\frac{\vartheta^2}{x} \right)_A \right] (x_B - x_A)$$

For most purposes it is also sufficiently accurate to
assume a value of $\eta_H = 1.00$.

The axial-velocity distribution is obtained by first
solving for the differences of the parameter φ_2 along

the radius by use of equation (8). When a $\Delta\varphi_2$ distribution is known, the φ_2 variation that satisfies the equation of continuity

$$\int_{x_h^2}^{1.0} \rho_1\varphi_1 \, dx^2 = \int_{x_h^2}^{1.0} \rho_2\varphi_2 \, dx^2$$

can be determined. (See appendix B.) When a ϑ_2 distribution is known, the φ_2 distribution can be obtained directly. When it is required that the axial-velocity distribution of a particular rotor be calculated, a φ_2 distribution must be assumed and the corresponding ϑ_2 distribution calculated, until by successive approximation distributions of φ_2 and ϑ_2 are obtained that satisfy all boundary and flow conditions. Usually only three calculations are necessary, and the labor is by no means prohibitive.

The axial-velocity-distribution equation for three-dimensional flow through a frictionless stator may be determined by setting $\omega = 0$ in equation (7) as follows:

$$\varphi_{2_B}^2 - \varphi_{2_A}^2 = \left(\varphi_{1_B}^2 - \varphi_{1_A}^2\right) + \left(\vartheta_{1_B}^2 - \vartheta_{1_A}^2\right) - \left(\vartheta_{2_B}^2 - \vartheta_{2_A}^2\right)$$

$$+ 2\int_{r_A}^{r_B} \frac{\vartheta_1^2}{x} \, dx - 2\int_{r_A}^{r_B} \frac{\vartheta_2^2}{x} \, dx$$

The value of ω used in the dimensionless parameters φ and ϑ in the foregoing equation may be that for the rotor used in conjunction with the stator. The actual velocity distribution is again found by satisfying the continuity relation.

APPENDIX B

ILLUSTRATIVE DESIGN OF A THREE-

DIMENSIONAL-FLOW ROTOR

In order to illustrate the use of the three-dimensional-flow equations of appendix A, a rotor with solid-body tangential-velocity distribution is designed. The flow is assumed to be incompressible and friction-less and the velocities upstream of the rotor are assumed to be uniform and axial. The following data are also assumed:

Hub-tip radius ratio $\left(x_h = \dfrac{r_h}{R}\right)$ 0.60

Axial velocity upstream of rotor, V_{a_1}, feet
    per second 200

Peripheral velocity of tip, ωR, feet
    per second 300

Hub tangential velocity downstream of rotor, u_{2_h},
    feet per second 90

Solidity $\left(\sigma = \dfrac{Bc}{2\pi r}\right)$ 1.0

The design computations are shown in table II.

The determination of the axial-velocity distribution is accomplished by using equation (8) of appendix A. For solid-body tangential-velocity distribution downstream of the rotor, uniform and axial entering velocities, and frictionless flow, equation (8) reduces to

$$\varphi_{2_B} - \varphi_{2_A} = \frac{1}{\varphi_1}\left[\left(x\vartheta_2\right)_B - \left(x\vartheta_2\right)_A - \left(\vartheta_{2_B}^2 - \vartheta_{2_A}^2\right)\right] \qquad (9)$$

since

$$\varphi_{2_B}{}^2 - \varphi_{2_A}{}^2 = \left(\varphi_{2_B} + \varphi_{2_A}\right)\left(\varphi_{2_B} - \varphi_{2_A}\right)$$

$$\approx 2\varphi_1\left(\varphi_{2_B} - \varphi_{2_A}\right)$$

and

$$2\int_{r_A}^{r_B} \frac{\vartheta_2{}^2}{x}\, dx = \vartheta_{2_B}{}^2 - \vartheta_{2_A}{}^2$$

The change in φ_2 is determined from equation (9) between the radial limits r_B and r_A corresponding to $x_B = 1.00$, $x_A = 0.80$, and $x_B = 0.80$, $x_A = 0.60$, respectively. The results are as follows:

$$x_B = 1.00 \qquad x_A = 0.80$$

$$\varphi_{2_B} - \varphi_{2_A} = 0.135$$

$$x_B = 0.80 \qquad x_A = 0.60$$

$$\varphi_{2_B} - \varphi_{2_A} = 0.105$$

A plot of $\Delta\varphi_2$ against x^2 is then made with $\Delta\varphi_2$ assumed equal to 0 at $x = 0.60$; and $\overline{\Delta\varphi_2}$ is determined by graphically evaluating the integral

$$\overline{\Delta\varphi_2} = \frac{1}{1 - x_h^2} \int_{x_h^2}^{1.0} \Delta\varphi_2 \ dx^2 \tag{10}$$

Values of φ_2 that satisfy the continuity relation are then determined at the three radii by use of the equation

$$\varphi_2 = \varphi_1 + \Delta\varphi_2 - \overline{\Delta\varphi_2} \tag{11}$$

Values of stagger angle β and turning angle θ that satisfy the required operating condition are found and the rotor performance is calculated. The blade sections were selected from the design charts of the NACA 65-series blower-blade sections (reference 3).

APPENDIX C

INCREASE OF TOTAL-PRESSURE RISE OBTAINABLE WITH SOLID-BODY

AND CONSTANT-TANGENTIAL-VELOCITY ROTORS

The weighted average total-pressure rise obtained with a rotor having uniform axial entering flow is, if frictionless incompressible flow is assumed,

$$\overline{\Delta H} = \frac{1}{Q} \int^{Q} \rho \omega r u_2 \ dQ = \frac{2\pi\rho\omega}{Q} \int_{r_h}^{R} r^2 u_2 V_{a_2} \ dr \qquad (12)$$

For a free-vortex loaded constant-flow-area rotor

$$u_2 = \frac{\text{Constant}}{r} = \frac{u_{2_h} r_h}{r}$$

$$V_{a_2} = V_{a_1} = \text{Constant}$$

Substituting in equation (12) leads to

$$\overline{\Delta H}_{\text{free-vortex}} = \frac{2\pi\rho\omega V_{a_1} u_{2_h} r_h}{Q} \int_{r_h}^{R} r \ dr$$

$$= \frac{\pi R^3 \rho \omega V_{a_1} u_{2_h} x_h}{Q} \left(1 - x_h^2\right)$$

$$= \rho \omega u_{2_h} R x_h \qquad (13)$$

An expression for the total-pressure rise obtainable with a rotor loaded in the solid-body manner is determined by substituting in equation (12) the following:

$$u_2 = \text{Constant} \times r$$

$$= \frac{u_{2_h}}{r_h} r$$

Thus

$$\overline{\Delta H}_{\text{solid-body}} = \frac{2\pi\rho\omega u_{2_h}}{Q r_h} \int_{r_h}^{R} r^3 V_{a_2} \, dr \qquad (14)$$

The integral in equation (14) may be evaluated by determining the V_{a_2} distribution for a particular rotor from equation (9) in appendix B. Equation (14) may be evaluated approximately by considering

$$V_{a_2} = V_{a_1} = \text{Constant}$$

or

$$\overline{\Delta H}_{\text{solid-body}} \approx \frac{2\pi\rho\omega V_{a_1} u_{2_h}}{Q r_h} \int_{r_h}^{R} r^3 \, dr$$

$$\approx \frac{\pi R^3 \rho\omega V_{a_1} u_{2_h}}{2 Q x_h} \left(1 - x_h^4\right)$$

$$\approx \frac{\rho\omega u_{2_h} R \left(1 + x_h^2\right)}{2 x_h} \qquad (15)$$

The ratio of the total-pressure rise obtainable with a solid-body rotor to the total-pressure rise obtainable with a corresponding free-vortex rotor with the same tangential velocity at the hub is approximately

$$\frac{\overline{\Delta H}_{\text{solid-body}}}{\overline{\Delta H}_{\text{free-vortex}}} \approx \frac{1 + x_h^2}{2x_h^2} \tag{16}$$

Similarly, the energy rise obtained with a constant-tangential-velocity rotor is approximately

$$\overline{\Delta H}_{u_2 = \text{Constant}} \approx \frac{2}{3} \frac{\pi R^3 \rho \omega V_{a_1} u_{2_h}}{Q} \left(1 - x_h^3\right)$$

$$\approx \frac{2}{3} \rho \omega u_{2_h} R \frac{1 - x_h^3}{1 - x_h^2}$$

and the ratio of energy rise is

$$\frac{\overline{\Delta H}_{u_2 = \text{Constant}}}{\overline{\Delta H}_{\text{free-vortex}}} \approx \frac{2\left(1 - x_h^3\right)}{3x_h\left(1 - x_h^2\right)} \tag{17}$$

REFERENCES

1. Bogdonoff, Seymour M., and Herrig, L. Joseph:
     Performance of Axial-Flow Fan and Compressor
     Blades Designed for High Loadings.
     NACA TN No. 1201, 1947.

2. Ruden, P.: Investigation of Single Stage Axial
     Fans. NACA TM No. 1062, 1944.

3. Bogdonoff, Seymour M., and Bogdonoff, Harriet E.:
     Blade Design Data for Axial-Flow Fans and Compressors.
     NACA ACR No. L5F07a, 1945.

4. Bell, E. Barton, and DeKoster, Lucas J.: Test of a
     Dual-Rotation Axial-Flow Fan. NACA ARR, Dec, 1942.

5. Bogdonoff, Seymour M., and Hess, Eugene E.: Axial-
     Flow Fan and Compressor Blade Design Data at 52.5°
     Stagger and Further Verification of Cascade Data
     by Rotor Tests. NACA TN No. 1271, 1947.

TABLE I

BLADE SECTION ORDINATES

NACA 65-(5.5)10 blower-blade section

Upper surface		Lower surface	
Station (in.)	Ordinate (in.)	Station (in.)	Ordinate (in.)
0.008	0.020	0.016	-0.014
.013	.025	.022	-.016
.024	.032	.034	-.019
.052	.048	.064	-.024
.109	.071	.123	-.031
.167	.090	.181	-.035
.225	.105	.239	-.039
.341	.130	.355	-.044
.458	.148	.470	-.047
.575	.163	.585	-.049
.692	.174	.700	-.050
.809	.181	.815	-.050
.926	.186	.930	-.049
1.043	.187	1.045	-.047
1.160	.183	1.160	-.043
1.277	.176	1.275	-.036
1.394	.165	1.390	-.028
1.510	.150	1.506	-.018
1.627	.132	1.621	-.008
1.743	.114	1.731	0
1.859	.094	1.853	.008
1.974	.072	1.970	.014
2.090	.050	2.086	.016
2.205	.028	2.203	.012
2.321	.003	2.319	-.003

L.E. radius: 0.015   T.E. radius: 0.003

NACA 65-(7.5)10 blower-blade section

Upper surface		Lower surface	
Station (in.)	Ordinate (in.)	Station (in.)	Ordinate (in.)
0.006	0.021	0.017	-0.012
.012	.026	.023	-.014
.022	.035	.036	-.016
.050	.052	.066	-.019
.107	.078	.125	-.023
.165	.099	.183	-.025
.223	.117	.241	-.027
.339	.145	.357	-.028
.456	.167	.472	-.028
.573	.184	.587	-.028
.690	.196	.702	-.027
.808	.205	.816	-.026
.925	.210	.931	-.024
1.043	.212	1.045	-.021
1.160	.209	1.160	-.017
1.277	.201	1.275	-.011
1.394	.189	1.390	-.003
1.511	.174	1.505	.006
1.628	.155	1.620	.014
1.744	.135	1.736	.021
1.860	.112	1.852	.027
1.975	.087	1.969	.030
2.090	.062	2.086	.028
2.205	.036	2.203	.019
2.321	.003	2.319	-.003

L.E. radius: 0.015   T.E. radius: 0.003

NACA 65-(9.5)10 blower-blade section

Upper surface		Lower surface	
Station (in.)	Ordinate (in.)	Station (in.)	Ordinate (in.)
0.005	0.022	0.018	-0.011
.010	.027	.025	-.012
.021	.037	.037	-.013
.048	.056	.068	-.015
.105	.085	.127	-.015
.162	.108	.186	-.015
.220	.128	.244	-.014
.337	.160	.359	-.012
.454	.185	.474	-.010
.571	.204	.589	-.007
.689	.219	.703	-.005
.807	.229	.817	-.002
.924	.235	.932	.001
1.042	.237	1.046	.004
1.160	.235	1.160	.009
1.278	.227	1.274	.015
1.395	.214	1.389	.022
1.512	.198	1.504	.029
1.629	.177	1.619	.037
1.745	.155	1.735	.042
1.860	.130	1.852	.045
1.976	.103	1.968	.045
2.091	.074	2.085	.040
2.206	.043	2.202	.027
2.321	.003	2.319	-.003

L.E. radius: 0.015   T.E. radius: 0.003

NACA 65-(12)10 blower blade-section

Upper surface		Lower surface	
Station (in.)	Ordinate (in.)	Station (in.)	Ordinate (in.)
0.004	0.023	0.019	-0.009
.009	.028	.026	-.009
.019	.039	.039	-.009
.046	.060	.070	-.009
.102	.094	.130	-.002
.217	.143	.247	.001
.334	.179	.362	.008
.452	.208	.477	.014
.569	.230	.591	.019
.687	.247	.705	.024
.805	.259	.819	.028
.923	.266	.933	.032
1.042	.269	1.046	.036
1.160	.267	1.160	.041
1.278	.258	1.274	.046
1.396	.245	1.388	.053
1.513	.227	1.503	.059
1.630	.206	1.618	.065
1.746	.181	1.734	.063
1.862	.153	1.850	.068
1.977	.122	1.967	.065
2.092	.089	2.084	.055
2.206	.052	2.202	.036
2.322	.003	2.318	-.003

L.E. radius: 0.015   T.E. radius: 0.003

TABLE II

ILLUSTRATIVE ROTOR DESIGN

Item	Source	Calculated values		
(1) $x = \dfrac{r}{R}$	Specified	0.60	0.80	1.00
(2) $\vartheta_2 = \dfrac{u_2}{\omega R}$	$\vartheta_2 = \dfrac{\vartheta_{2_h}}{x_h} x$	.30	.40	.50
(3) $\varphi_1 = \dfrac{V_{a_1}}{\omega R}$	Specified	.667	.667	.667
(4) $\Delta\varphi_2$	Equation (9)	0	.105	.240
(5) $\overline{\Delta\varphi_2}$	Equation (10)	.120	.120	.120
(6) $\varphi_2 = \dfrac{V_{a_2}}{\omega R}$	Equation (11)	.547	.652	.787
(7) $\varphi = \dfrac{V_a}{\omega R} = \dfrac{\varphi_1 + \varphi_2}{2}$	$\dfrac{\text{Item (3) + Item (6)}}{2}$	.607	.659	.727
(8) $\tan \beta = \dfrac{x}{\varphi}$	$\dfrac{\text{Item (1)}}{\text{Item (7)}}$	.988	1.213	1.374
(9) $\tan (\beta - \theta)$ $= \tan \beta - \dfrac{\vartheta^2}{\varphi}$	Item (8) - $\dfrac{\text{Item (2)}}{\text{Item (7)}}$	.494	.606	.686
(10) $\Delta p/q_a$	Equation (2)	1.121	1.156	1.089
(11) $\Delta H/q_a$	Equation (3)	.975	1.476	1.892
(12) $\Delta p/q_{a_1}$	Item (10) $\dfrac{\text{Item (7)}^2}{\text{Item (3)}^2}$	.93	1.13	1.29
(13) $\Delta H/q_{a_1}$	Item (11) $\dfrac{\text{Item (7)}^2}{\text{Item (3)}^2}$	0.81	1.44	2.25
(14) β, deg	$\tan^{-1}$ Item (8)	44.6	50.5	54.0
(15) θ, deg	Item (14) - $\tan^{-1}$ Item (9)	18.3	19.3	19.6
(16) $\sigma = \dfrac{Bc}{2\pi r}$	Specified	1.0	1.0	1.0
(17) Design camber of NACA 65-series blower-blade sections	Items (14), (15), (16), fig. 41(a) of reference 3	1.00	1.20	1.25
(18) α, deg	Items (14), (16), (17), fig. 41(b) of reference 3	13.5	14.8	15.2
(19) Blade angle, deg	Item (18) + (90 - Item (14))	58.9	54.3	51.2

NATIONAL ADVISORY
COMMITTEE FOR AERONAUTICS

(a) Flow streamlines.

(b) Axial-velocity profiles.

Figure 1.- Flow streamlines and axial-velocity profiles in
three-dimensional frictionless flow through a rotor.

Fig. 2   NACA RM No. L7D02a
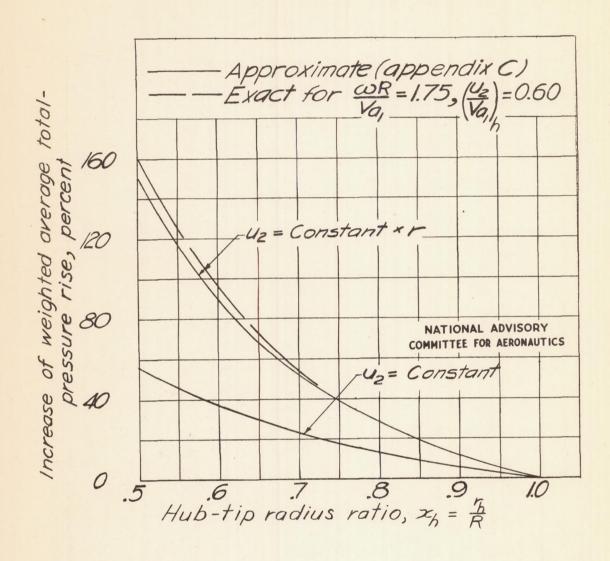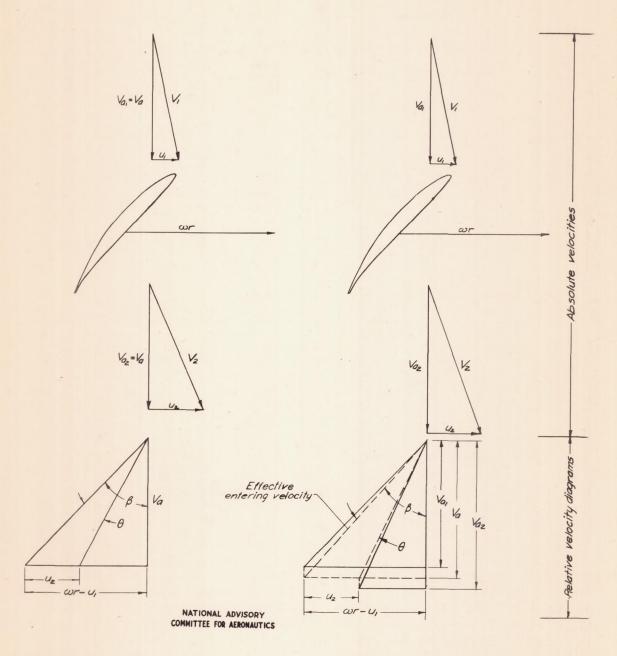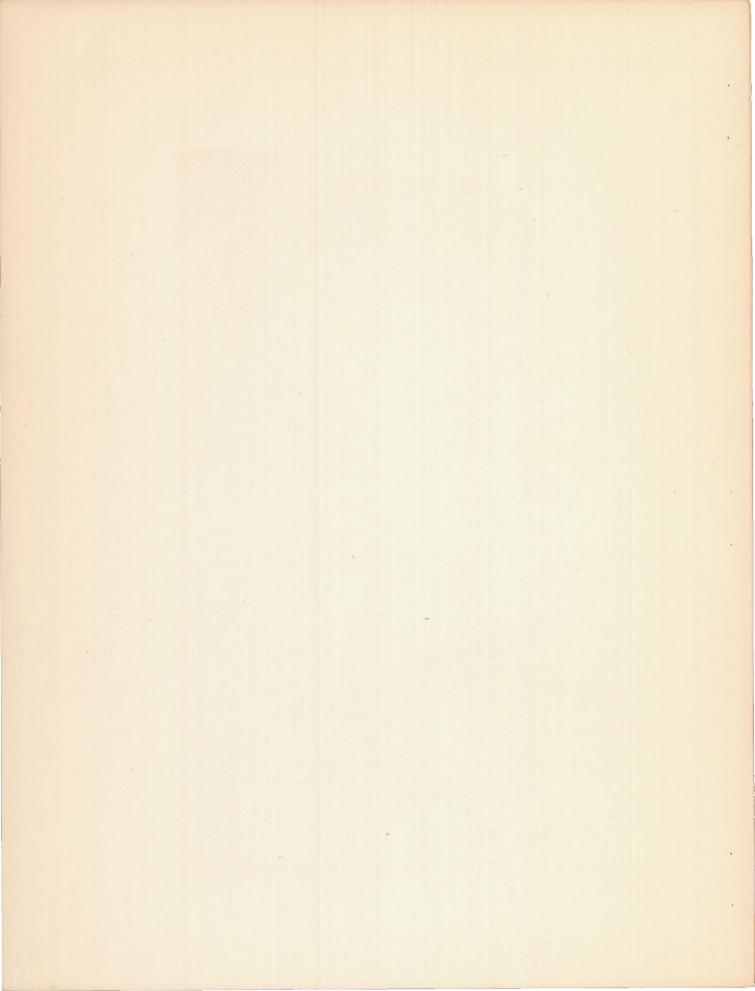
Figure 2.- Increase of total-pressure rise obtainable with
    rotors having solid-body and uniform tangential-velocity
    distributions as compared with total-pressure rise obtain-
    able with free-vortex loaded rotor. The same tangential-
    velocity parameter at the hub is assumed for all three
    rotors.

(a) Constant axial velocity.   (b) Varying axial velocity.
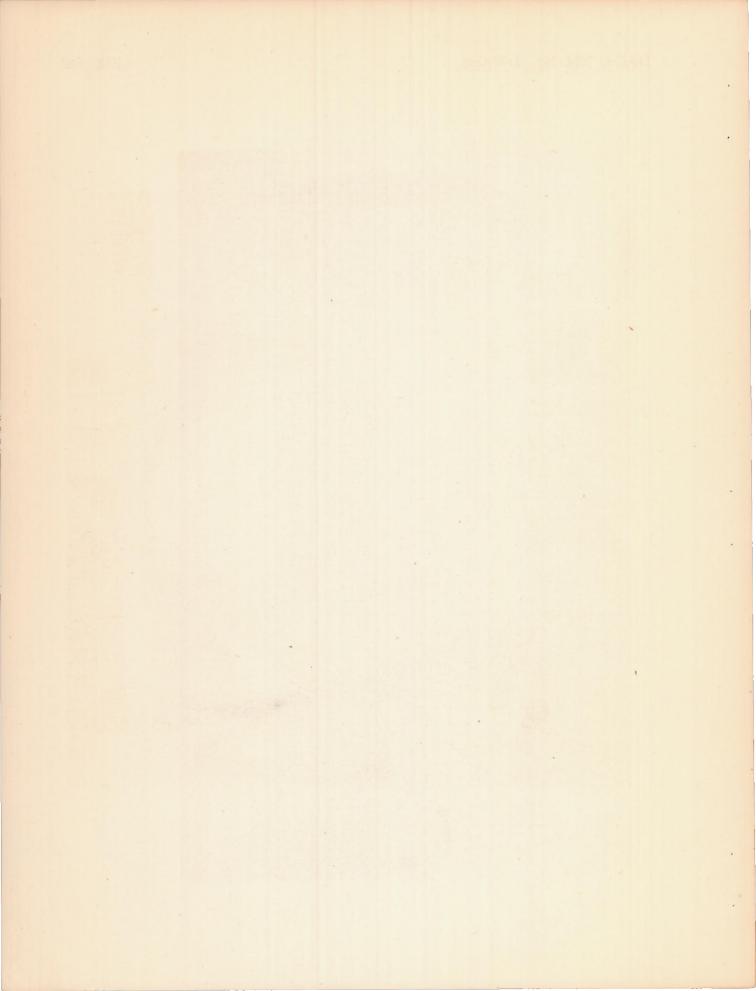
Figure 3.- Typical rotor velocity diagrams.
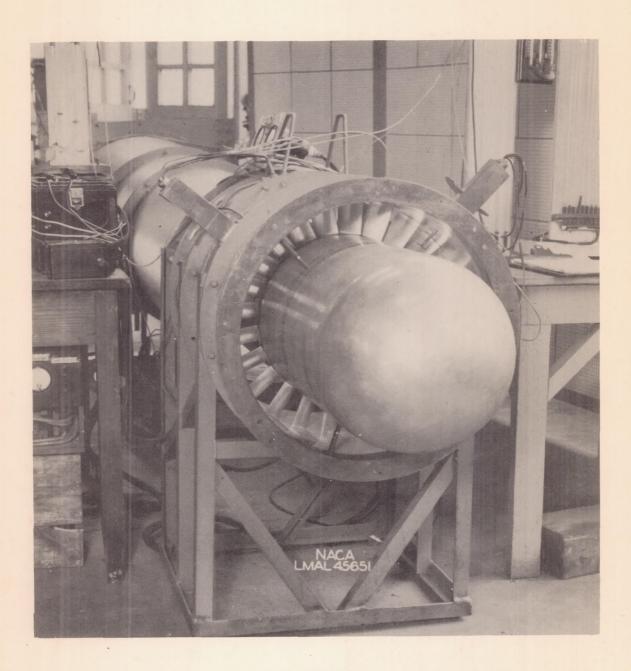
(a) Complete test setup.

Figure 4.- Views of test arrangement from entrance end.

(b) Entrance removed.

Figure 4.- Concluded.
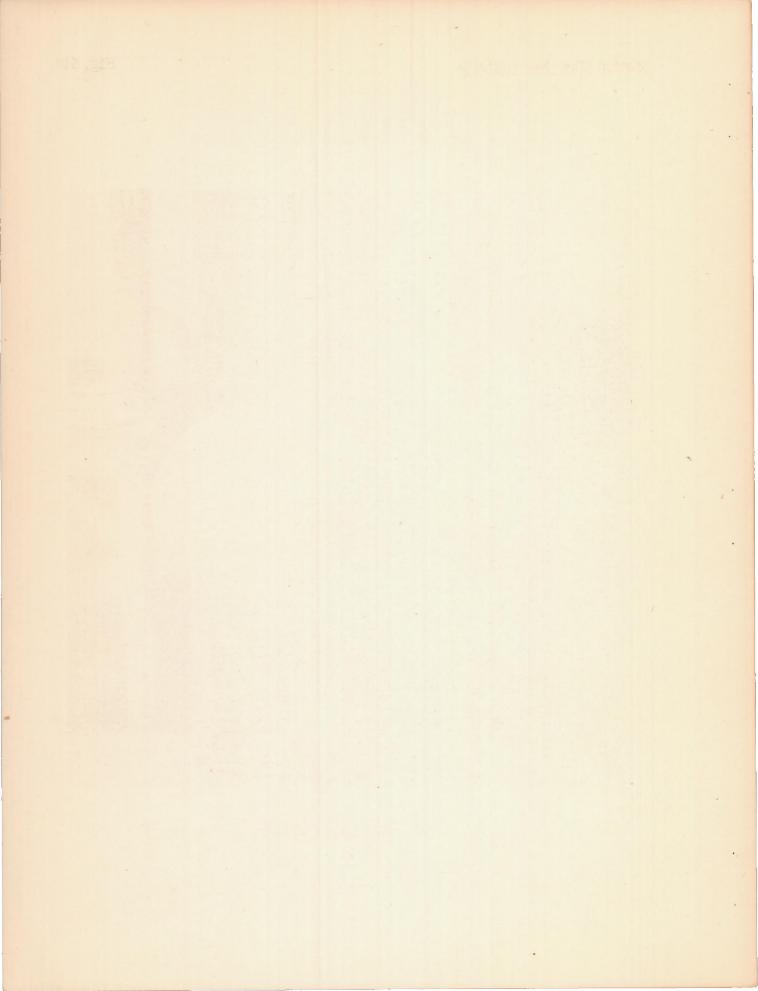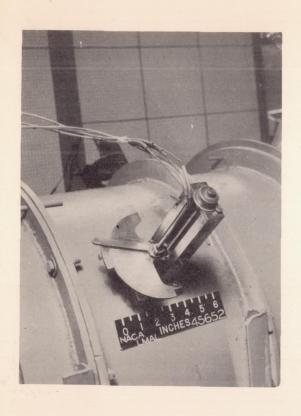
Figure 5.- Schematic drawing of test arrangement.

**NATIONAL ADVISORY
COMMITTEE FOR AERONAUTICS**

Fig. 5
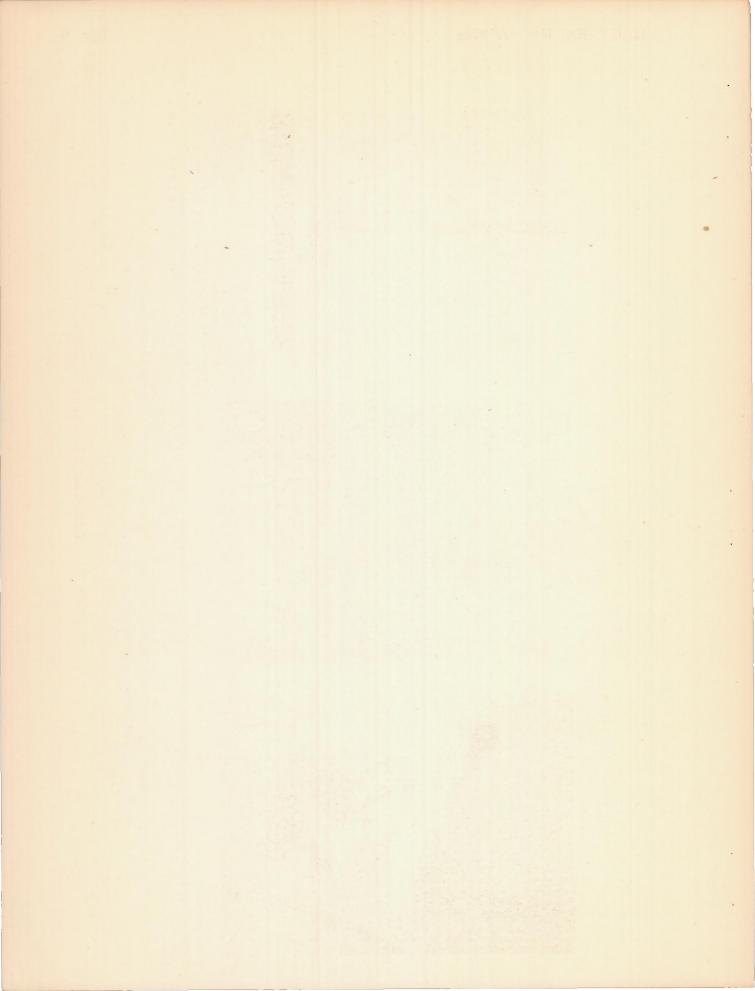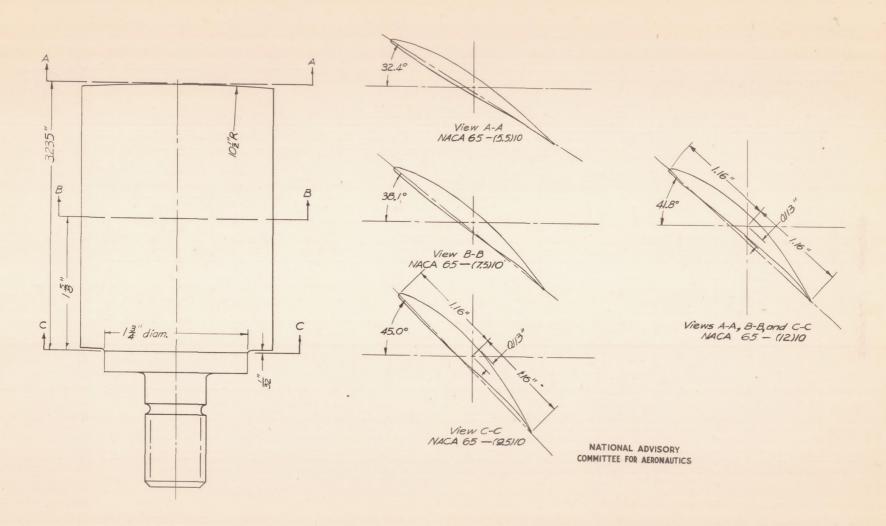
(a) External view.　　　　(b) Survey tube in duct.　　(c) Detail view of survey tube.

Figure 6.- Views of survey instruments.

Fig. 6
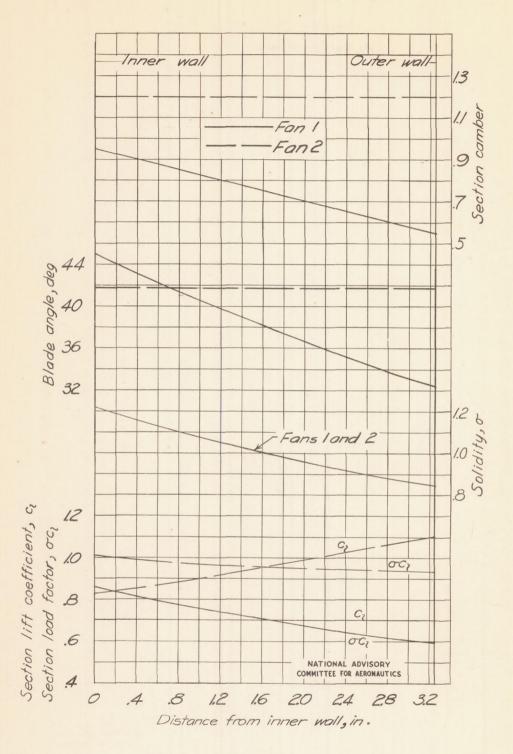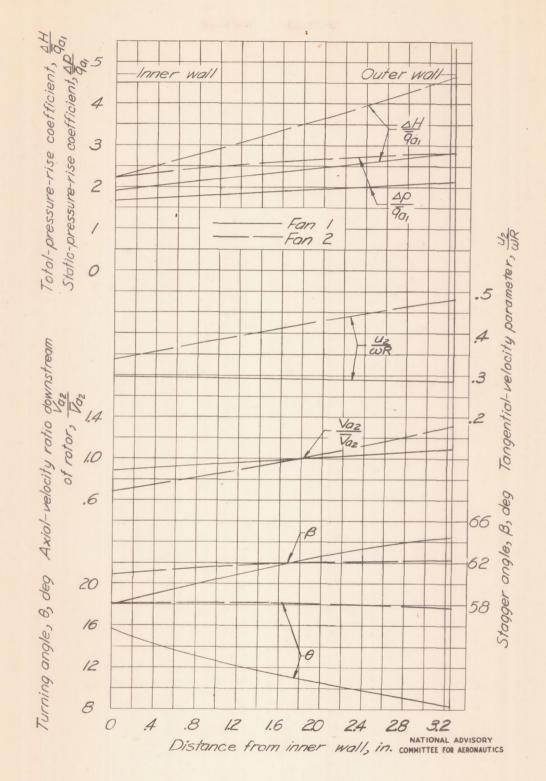
(a) Plan form.   (b) Fan 1 blade sections.   (c) Fan 2 blade section.

Figure 7.- Drawing of rotor blades.

Fig. 7

(a) Blade characteristics.

Figure 8.- Blade and theoretical performance characteristics
of test rotors.

(b) Theoretical performance characteristics.

Figure 8.- Concluded.

Fig. 9

(a) Fan 1.

(b) Fans 2 and 2a.
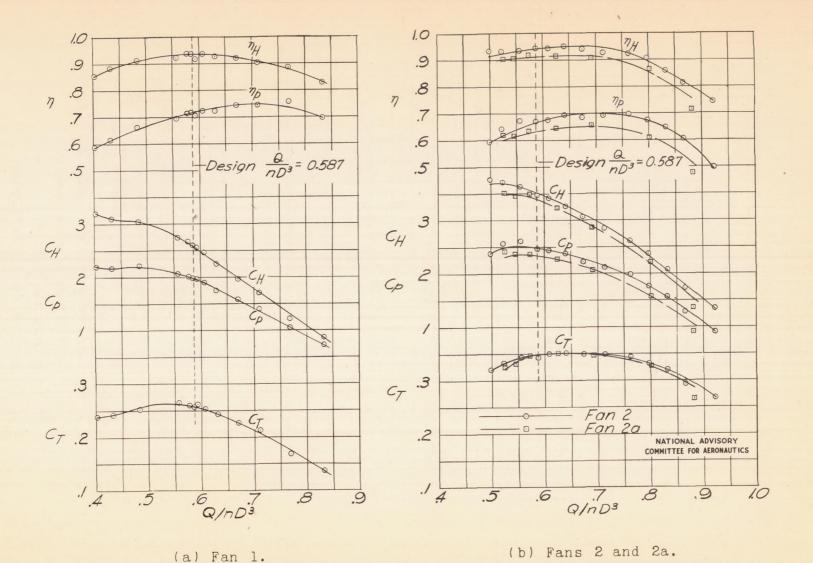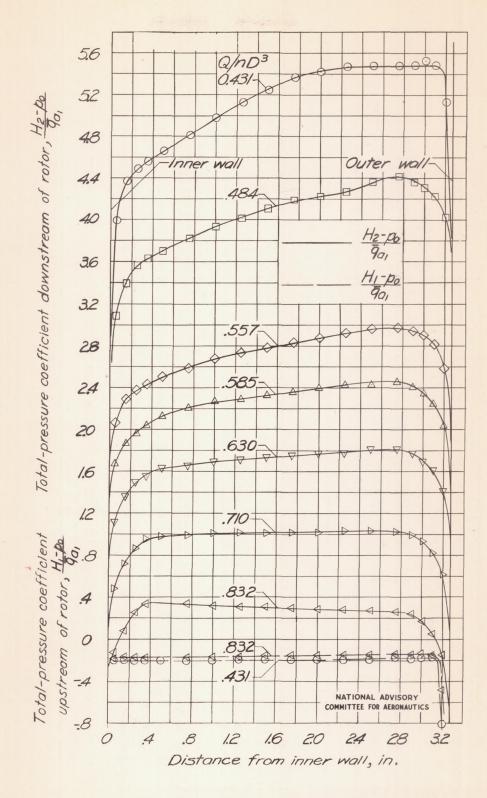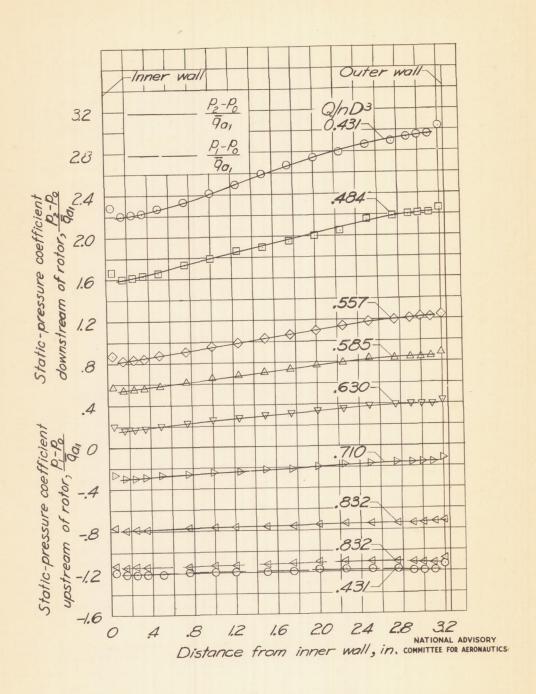
Figure 9.- Over-all characteristic curves of fans 1, 2, and 2a.

(a) Total-pressure coefficient.

Figure 10.- Fan 1 survey results. Design $\dfrac{Q}{nD^3} = 0.587$.

(b) Static-pressure coefficient.

Figure 10.- Continued. Fan 1.

(c) Tangential-velocity parameter downstream of rotor.

(d) Axial-velocity ratio downstream of rotor.
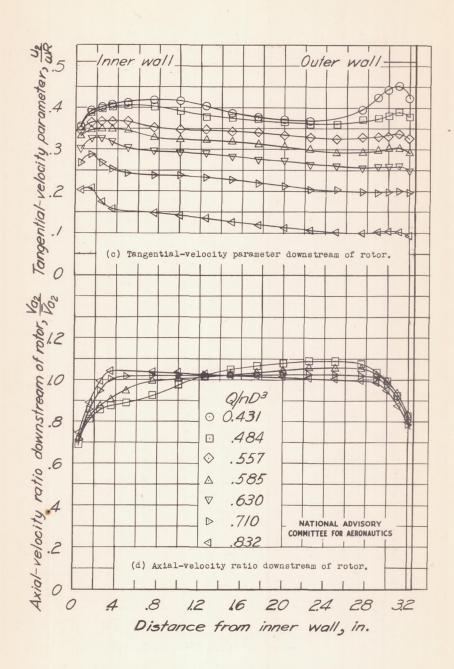
Figure 10.- Continued. Fan 1.

Figure 10.- Concluded. Fan 1.
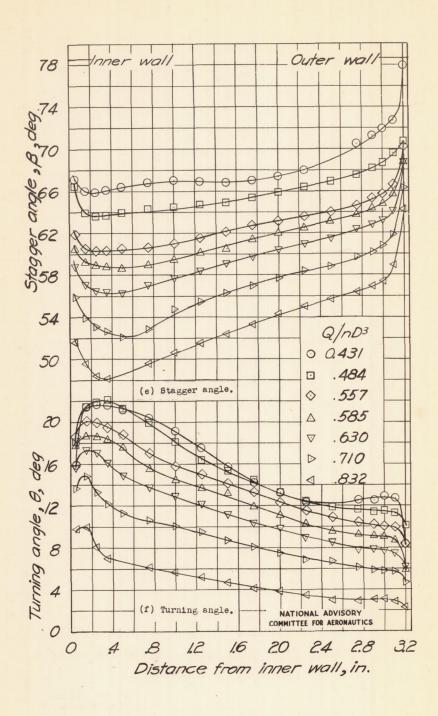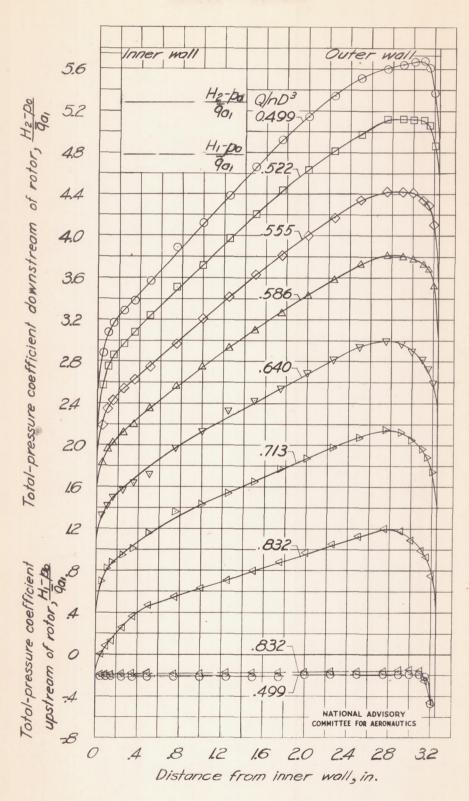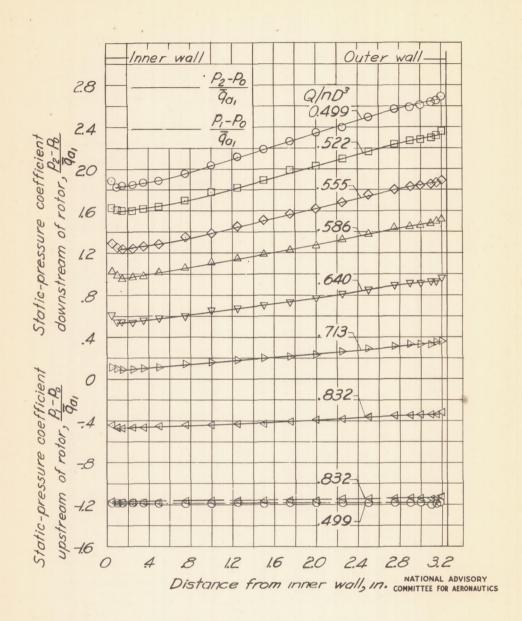
(a) Total-pressure coefficient.

Figure 11.- Fan 2 survey results. Design $\dfrac{Q}{nD^3} = 0.587$.

(b) Static-pressure coefficient.

Figure 11.- Continued. Fan 2.

(c) Tangential-velocity parameter downstream of rotor.

(d) Axial-velocity ratio downstream of rotor.

$$Q/nD^3$$

⊙ 0.499
□ .522
◇ .555
△ .586
▽ .640
▷ .713
◁ .832

Inner wall   Outer wall

Tangential-velocity parameter, $\frac{u_2}{wR}$

Axial-velocity ratio downstream of rotor, $\frac{Va_2}{\overline{Va_2}}$

Distance from inner wall, in.
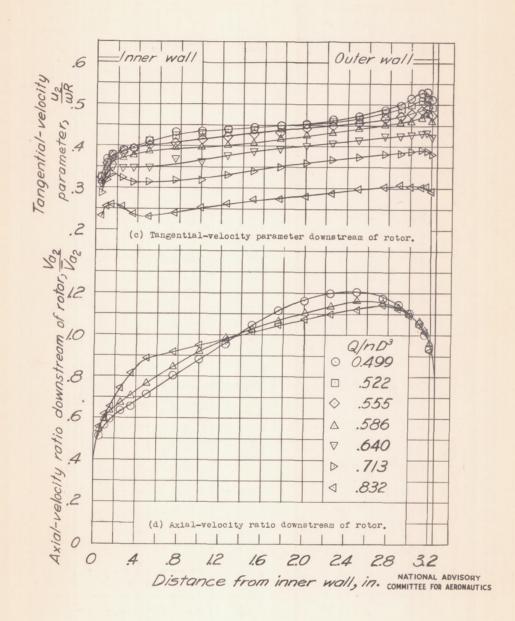
Figure 11.- Continued. Fan 2.

Figure 11.- Concluded. Fan 2.
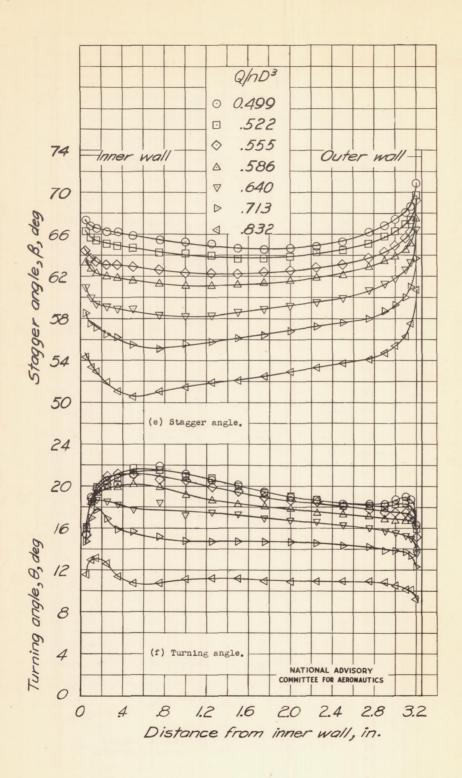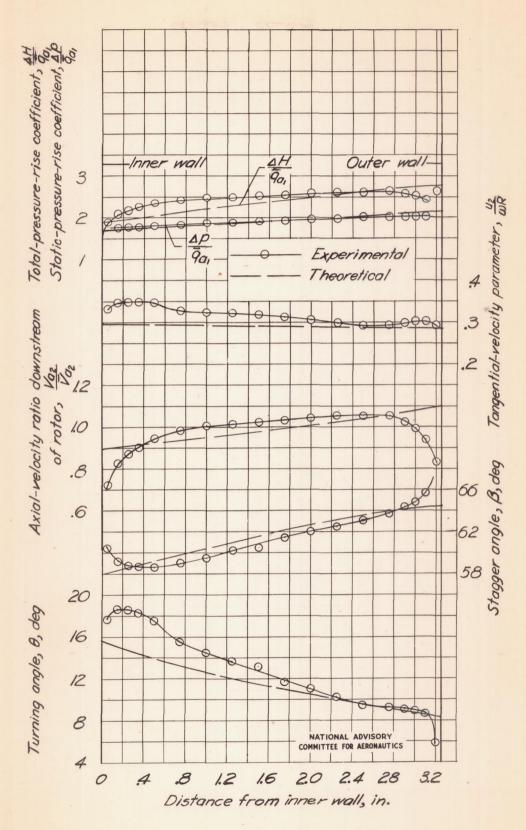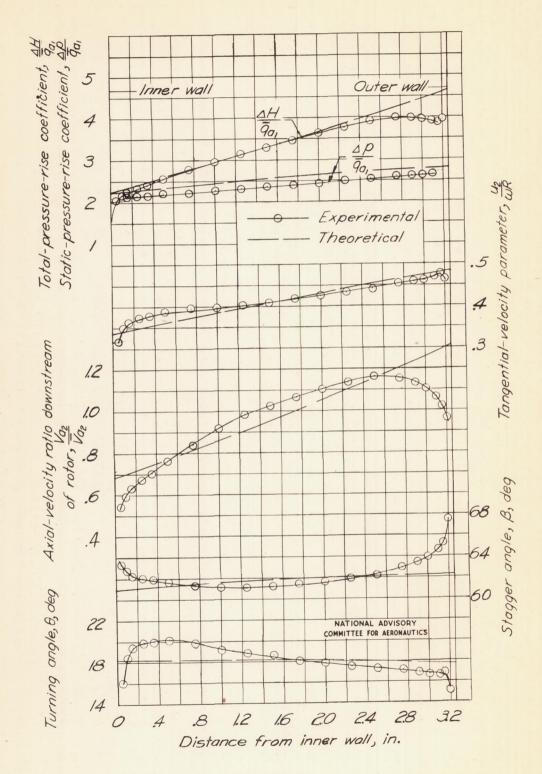
(a) Fan 1.

Figure 12.- Comparison of experimental surveys with
theory at design point.

(b) Fan 2.

Figure 12.- Concluded.
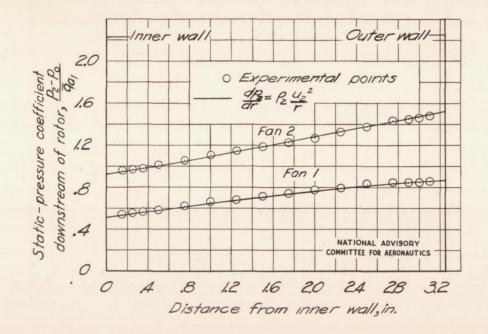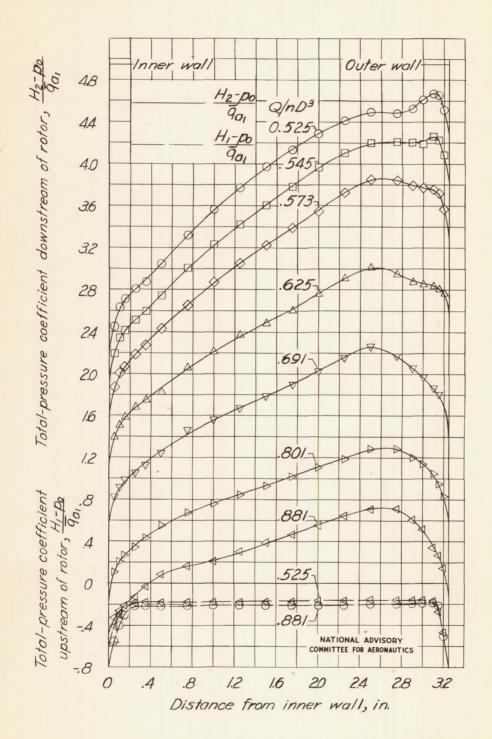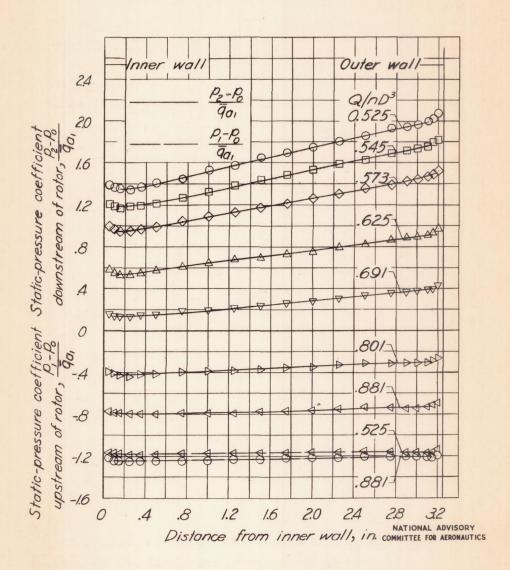
Figure 13.- Comparison of experimental and theoretical
static-pressure gradients downstream of rotor.

Fig. 13

(a) Total-pressure coefficient.

Figure 14.- Fan 2a survey results.

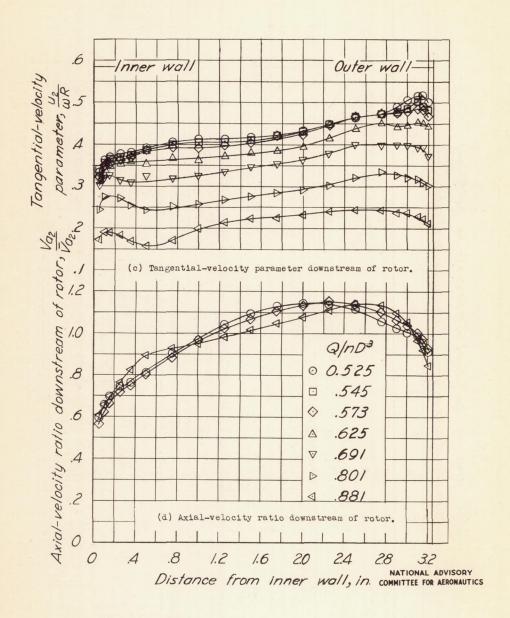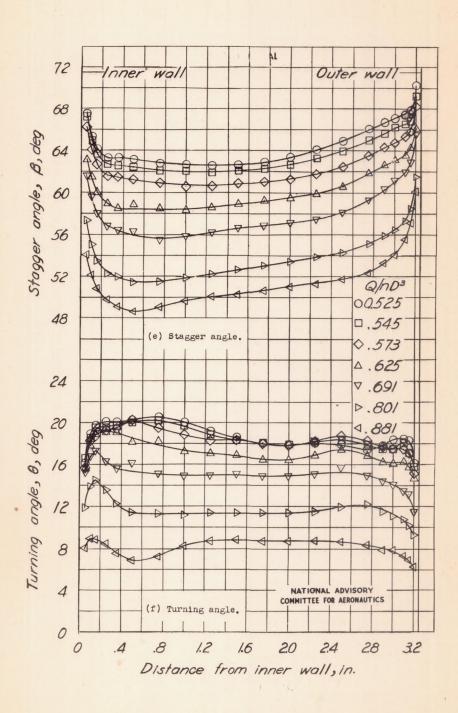(b) Static-pressure coefficient.

Figure 14.- Continued. Fan 2a.

(c) Tangential-velocity parameter downstream of rotor.

(d) Axial-velocity ratio downstream of rotor.

Q/nD^3

⊙ 0.525
☐   .545
◇   .573
△   .625
▽   .691
▷   .801
◁   .881

Figure 14.- Continued. Fan 2a.

Figure 14.- Concluded. Fan 2a.

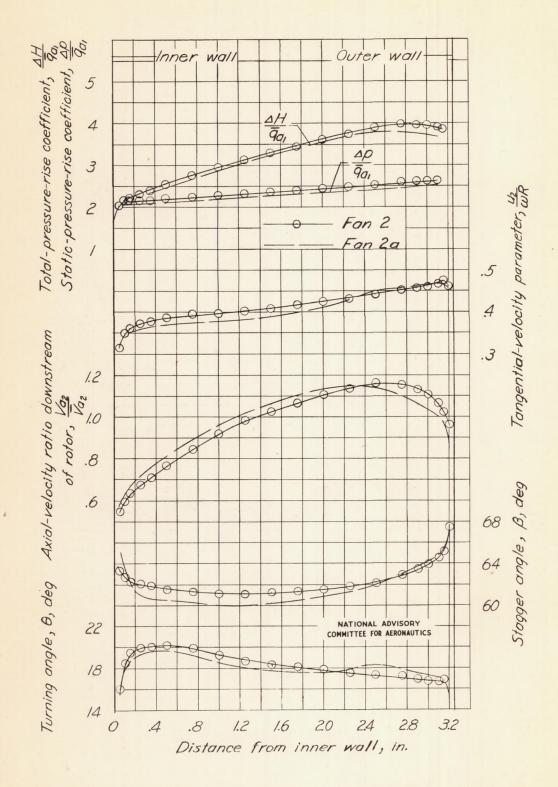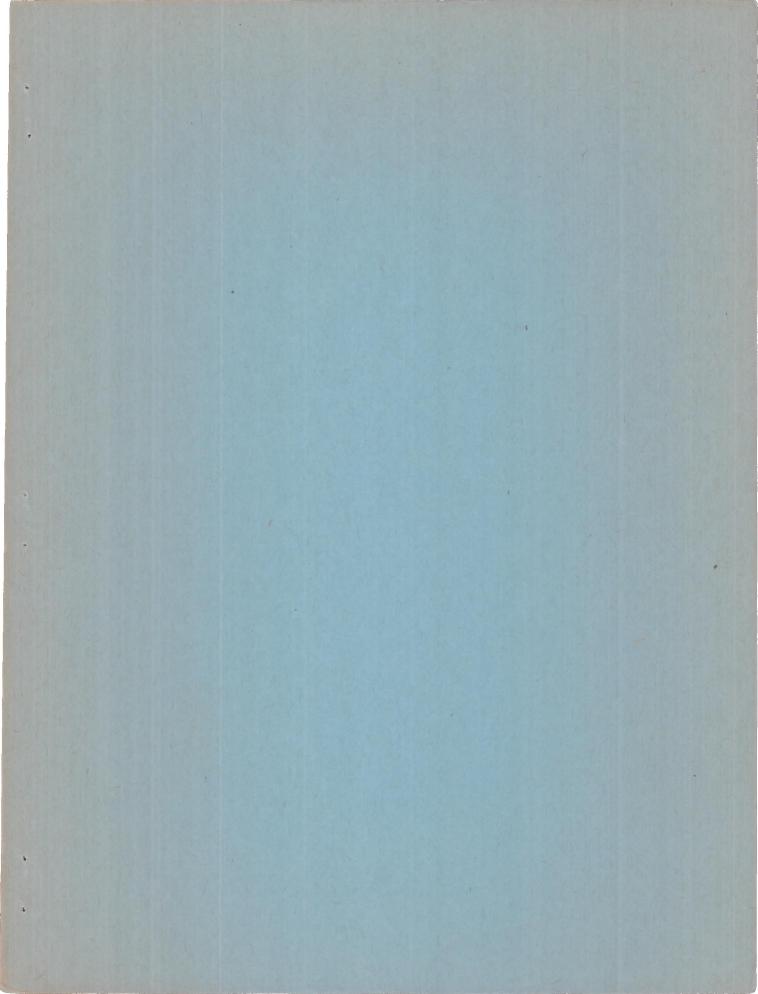Fig. 15   NACA RM No. L7D02a

Figure 15.- Comparison of fan 2 and 2a survey results
at $\dfrac{Q}{nD^3}$ = 0.586.